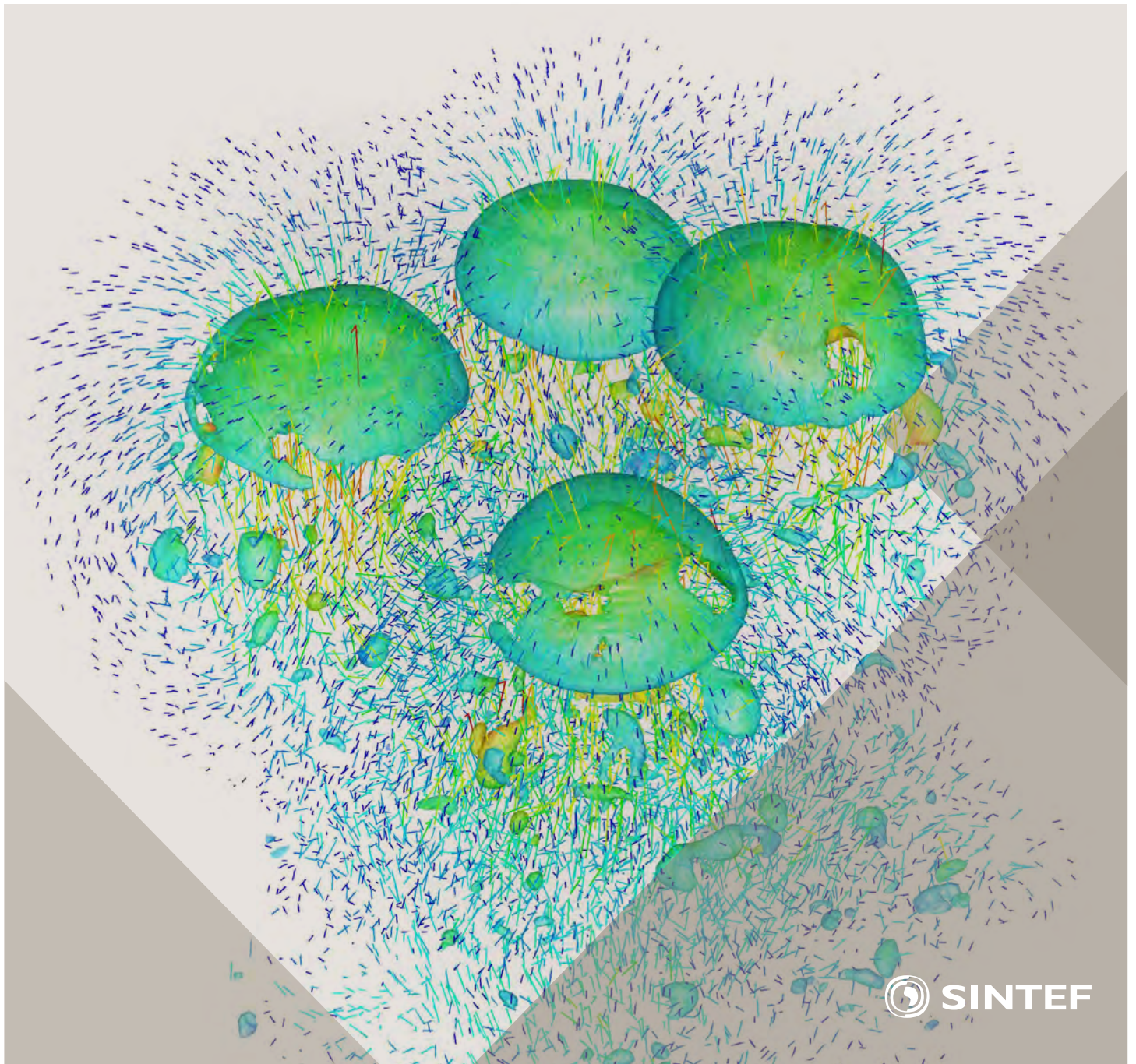


Selected papers from 10th International Conference on
Computational Fluid Dynamics in the Oil & Gas, Metal-
lurgical and Process Industries

Progress in Applied CFD



SINTEF Proceedings

Editors:

Jan Erik Olsen and Stein Tore Johansen

Progress in Applied CFD

Selected papers from 10th International Conference on Computational Fluid
Dynamics in the Oil & Gas, Metallurgical and Process Industries

SINTEF Academic Press

SINTEF Proceedings no 1

Editors: Jan Erik Olsen and Stein Tore Johansen

Progress in Applied CFD

Selected papers from 10th International Conference on Computational Fluid Dynamics in the Oil & Gas, Metallurgical and Process Industries

Key words:

CFD, Flow, Modelling

Cover, illustration: Rising bubbles by Schalk Cloete

ISSN 2387-4287 (printed)

ISSN 2387-4295 (online)

ISBN 978-82-536-1432-8 (printed)

ISBN 978-82-536-1433-5 (pdf)

60 copies printed by AIT AS e-dit

Content: 100 g munken polar

Cover: 240 g trucard

© Copyright SINTEF Academic Press 2015

The material in this publication is covered by the provisions of the Norwegian Copyright Act. Without any special agreement with SINTEF Academic Press, any copying and making available of the material is only allowed to the extent that this is permitted by law or allowed through an agreement with Kopinor, the Reproduction Rights Organisation for Norway. Any use contrary to legislation or an agreement may lead to a liability for damages and confiscation, and may be punished by fines or imprisonment

SINTEF Academic Press

Address: Forskningsveien 3 B
 PO Box 124 Blindern
 N-0314 OSLO

Tel: +47 22 96 55 55

Fax: +47 22 96 55 08

www.sintef.no/byggforsk

www.sintefbok.no

SINTEF Proceedings

SINTEF Proceedings is a serial publication for peer-reviewed conference proceedings on a variety of scientific topics.

The processes of peer-reviewing of papers published in SINTEF Proceedings are administered by the conference organizers and proceedings editors. Detailed procedures will vary according to custom and practice in each scientific community.

PREFACE

This book contains selected papers from the 10th International Conference on Computational Fluid Dynamics in the Oil & Gas, Metallurgical and Process Industries. The conference was hosted by SINTEF in Trondheim in June 2014 and is also known as CFD2014 for short. The conference series was initiated by CSIRO and Phil Schwarz in 1997. So far the conference has been alternating between CSIRO in Melbourne and SINTEF in Trondheim. The conferences focus on the application of CFD in the oil and gas industries, metal production, mineral processing, power generation, chemicals and other process industries. The papers in the conference proceedings and this book demonstrate the current progress in applied CFD.

The conference papers undergo a review process involving two experts. Only papers accepted by the reviewers are presented in the conference proceedings. More than 100 papers were presented at the conference. Of these papers, 27 were chosen for this book and reviewed once more before being approved. These are well received papers fitting the scope of the book which has a slightly more focused scope than the conference. As many other good papers were presented at the conference, the interested reader is also encouraged to study the proceedings of the conference.

The organizing committee would like to thank everyone who has helped with paper review, those who promoted the conference and all authors who have submitted scientific contributions. We are also grateful for the support from the conference sponsors: FACE (the multiphase flow assurance centre), Total, ANSYS, CD-Adapco, Ascomp, Statoil and Elkem.

Stein Tore Johansen & Jan Erik Olsen



Organizing committee:

Conference chairman: Prof. Stein Tore Johansen
Conference coordinator: Dr. Jan Erik Olsen
Dr. Kristian Etienne Einarsrud
Dr. Shahriar Amini
Dr. Ernst Meese
Dr. Paal Skjetne
Dr. Martin Larsson
Dr. Peter Witt, CSIRO

Scientific committee:

J.A.M. Kuipers, TU Eindhoven
Olivier Simonin, IMFT/INP Toulouse
Akio Tomiyama, Kobe University
Sanjoy Banerjee, City College of New York
Phil Schwarz, CSIRO
Harald Laux, Osram
Josip Zoric, SINTEF
Jos Derksen, University of Aberdeen
Dieter Bothe, TU Darmstadt
Dmitry Eskin, Schlumberger
Djamel Lakehal, ASCOMP
Pär Jonsson, KTH
Ruben Shulkes, Statoil
Chris Thompson, Cranfield University
Jinghai Li, Chinese Academy of Science
Stefan Pirker, Johannes Kepler Univ.
Bernhard Müller, NTNU
Stein Tore Johansen, SINTEF
Markus Braun, ANSYS

CONTENTS

Chapter 1: Pragmatic Industrial Modelling	7
On pragmatism in industrial modeling	9
Pragmatic CFD modelling approaches to complex multiphase processes.....	25
A six chemical species CFD model of alumina reduction in a Hall-Héroult cell	39
Multi-scale process models to enable the embedding of CFD derived functions: Curtain drag in flighted rotary dryers	47
Chapter 2: Bubbles and Droplets	57
An enhanced front tracking method featuring volume conservative remeshing and mass transfer	59
Drop breakup modelling in turbulent flows	73
A Baseline model for monodisperse bubbly flows	83
Chapter 3: Fluidized Beds	93
Comparing Euler-Euler and Euler-Lagrange based modelling approaches for gas-particle flows.....	95
State of the art in mapping schemes for dilute and dense Euler-Lagrange simulations	103
The parametric sensitivity of fluidized bed reactor simulations carried out in different flow regimes.....	113
Hydrodynamic investigation into a novel IC-CLC reactor concept for power production with integrated CO ₂ capture	123
Chapter 4: Packed Beds	131
A multi-scale model for oxygen carrier selection and reactor design applied to packed bed chemical looping combustion	133
CFD simulations of flow in random packed beds of spheres and cylinders: analysis of the velocity field	143
Numerical model for flow in rocks composed of materials of different permeability.....	149
Chapter 5: Metallurgical Applications	157
Modelling argon injection in continuous casting of steel by the DPM+VOF technique.....	159
Modelling thermal effects in the molten iron bath of the HIs melt reduction vessel.....	169
Modelling of the Ferrosilicon furnace: effect of boundary conditions and burst	179
Multi-scale modeling of hydrocarbon injection into the blast furnace raceway.....	189
Prediction of mass transfer between liquid steel and slag at continuous casting mold	197
Chapter 6: Oil & Gas Applications	205
CFD modeling of oil-water separation efficiency in three-phase separators.....	207
Governing physics of shallow and deep subsea gas release	217
Cool down simulations of subsea equipment.....	223
Lattice Boltzmann simulations applied to understanding the stability of multiphase interfaces.....	231
Chapter 7: Pipeflow	239
CFD modelling of gas entrainment at a propagating slug front.....	241
CFD simulations of the two-phase flow of different mixtures in a closed system flow wheel.....	251
Modelling of particle transport and bed-formation in pipelines	259
Simulation of two-phase viscous oil flow	267

CFD SIMULATIONS OF THE TWO-PHASE FLOW OF DIFFERENT MIXTURES IN A CLOSED SYSTEM FLOW WHEEL

José F. ROCA R.^{1*}, João N.E. CARNEIRO¹, José E.S. OLIVEIRA¹, Sjur MO², Martin FOSSEN³,
 Stein T. JOHANSEN²

¹Instituto SINTEF do Brasil, 22251-050 Rio de Janeiro, BRAZIL

²SINTEF Materials and Chemistry, 7465 Trondheim, NORWAY

³SINTEF Petroleum Research, 7465 Trondheim, NORWAY

* E-mail: jose.roca@sintefbrasil.org.br

ABSTRACT

The objective of this work is to study the behaviour of mixtures involving air/water and oil/water at low pressures and oil/ high CO₂-content gas at high pressures in a closed system 'Wheel Flow Loop'. Such apparatus has been used in different contexts before, e.g. to evaluate the mixture apparent viscosity of different emulsions or the hydrate behaviour under realistic conditions of pressure and temperature. Typically, torque and rotation velocity measurements are used to estimate the overall wall shear stresses. Only in a few cases, there exists the possibility to visualize the interface between phases through a (sapphire) window. Furthermore, secondary flow present in such curved configurations may have an effect on pressure loss depending on ratio of pipe diameter and curvature radius and flow regime. Consequently, more detailed information on the flow and phase distribution in the wheel is very relevant to understand the underlying physics in the wheel and aid data interpretation.

In this paper, two-phase flow in the Wheel Flow Loop geometry is simulated numerically, by means of a classic Volume of Fluid (VOF) approach and a coupled 'VOF' / Eulerian-Eulerian approach. Thus, 3D flow calculations using ANSYS[®] Fluent's VOF are critically compared with a Quasi-3D (Q3D) approach from LedaFlow[®]. Additionally, both numerical results have been compared with experimental data obtained in the SINTEF Multiphase Flow Laboratory at Tiller in Norway for different mixtures showing reasonable agreement. Torque/velocity output data has received special attention.

Experiments have evidenced hysteretic behaviour when an increasing-decreasing stepwise angular velocity is imposed to the wheel. Both this phenomenon and the carry-over starting point have been successfully reproduced by the CFD calculations.

Keywords: Wheel flow loop, CO₂-rich mixture, two-phase flow, Quasi-3D.

NOMENCLATURE

Greek Symbols

ℓ Turbulent length scale, [m]
 λ Friction factor, [-]
 μ Dynamic viscosity, [Pa · s]
 ρ Mass density, [kg/m³]
 θ Polar coordinate (angle), [°]
 τ^{wall} Wall shear stress, [Pa]

Latin Symbols

a Pipe radius, [m]
 A^{wall} Wall area, [m²]
 d Pipe diameter, [m]
 De Dean number ($De = Re \sqrt{\frac{a}{R}}$), [-]
 GOR Gas-oil ratio, [m³/m³]
 k Turbulent kinetic energy, [m²/s²]
 LSI Large Scale Interface
 N_x Number of x -cells, [-]
 N_y Number of y -cells, [-]
 $Q3D$ Quasi-3D
 r Polar coordinate (radius), [m]
 R Wheel radius, [m]
 Re Reynolds number ($Re = \frac{\rho U_0^{\text{wall}} d}{\mu}$), [-]
 Re_c Critical Reynolds number, [-]
 t Time, [s]
 T Torque, [N · m]
 U^{wall} Wall velocity of the wheel, [m/s]
 x Streamwise coordinate, [m]
 y Transversal coordinate, [m]

Sub/superscripts

i x -index (streamwise)
 j y -index (transversal)

INTRODUCTION

During petroleum production gas, oil and water may flow simultaneously in pipes, forming complex mixtures which are often difficult to characterize under realistic conditions. A closed system wheel flow loop has been used by different authors (e.g. Urdahl et al., 1997; Johnsen et al., 2001; Johnsen and Rønningsen, 2003) as an approach to estimate the apparent viscosity of mixtures under different water cuts, realistic pressure - temperature conditions and Reynolds numbers as usually observed in the field. These are not straightforward to be reproduced, e.g. in standard rheometers. The idea behind such setting is that the wheel may, in some respect, resemble a pressurized infinite loop, being relatively easy to operate with reduced costs. This, and the possibility to place the wheel inside a climate chamber has also driven the use as a tool to study flow assurance problems, e.g. related to hydrates, including the performance of inhibitors (Rasch et al., 2001). An example of a wheel flow loop is shown in Figure 1.

Recently, the production and transport of hydrocarbon mixtures with high CO₂ content have received special attention (Zain et al., 2001; Almeida et al., 2010). The presence of CO₂ in unusual amounts may compromise mechanical integrity due to pipeline corrosion while influencing other issues related to flow assurance such as excessive Joule - Thomson cooling, wax deposition, inorganic scaling, among others. Experiments for such mixtures in flowing systems are very expensive and rarely found. Thus, the wheel setup has been also evaluated here for systems containing significant CO₂ content.

In one of the early works on flows in curved pipes, Mori and Nakayama (1964) studied the effect of curvature on secondary flows. Over a wide range of laminar- and turbulent regimes, they noted that fluid is driven to the outer wall by centrifugal forces creating vortices in the cross section as shown in Figure 2. In addition, they noticed that secondary flows create an extra flow resistance which depends on the ratio of the wheel to the pipe radii R/a affecting pressure drop for different regimes. Figure 3 depicts the friction factor λ as function of a wide range of Reynolds numbers Re . It was observed that the curvature effects is higher at laminar regimes than for turbulent flow. In fact, the diminution of curvature effect is even more evident at higher $Re \sim 10^4$. Furthermore, the critical Reynolds number Re_c , at which transition to turbulent flow occurs, increases as radii ratio R/a diminishes, i.e. when curvature effect augments.

White and Bond (1971) pointed out the advantage of using a small scale hollow shaped wheel for the estimation of friction factors of fluids containing high molecular weight species where shear degradation of the molecules can occur under conditions of high local shear stresses (e.g. in pumps or valves), otherwise present in standard flow loop configurations.

In the work of Urdahl et al.(1997) a closed wheel flow loop



Figure 1: Wheel Flow Loop located at the Tiller Laboratory, SINTEF Norway.

is used to evaluate the effective viscosity of live oil. The imposed rotation produces a relative velocity between fluid and pipe wall resembling transportation of the fluid in a pipe. They found that, at constant temperature, viscosity increases with higher velocities when mixing between oil- and water phase takes place. Johnsen et al.(2001) used also a rotating wheel to calculate the apparent viscosity of emulsion through measurements of torque at a wide range of tangential velocities ranging from 0.7 m/s to 3.0 m/s. They compared the results with data obtained from viscometers and traditional flow loops, finding reasonable agreement with emulsion of 50% – 60% water cut.

Johnsen and Rønningesen (2003) applied the wheel shaped loop to study water-in-oil emulsions with several live North Sea oils with saturation pressures up to 100 bar and water cuts up to 90%. The method is shown to provide useful estimates of emulsion viscosity for live oils.

Visualization of the flow in these types of experiments is usually limited. In this context, the present work is an attempt to better understand the flow phenomena inside the wheel through detailed CFD computations and comparison of Torque measurements. During the last decade SINTEF, ConocoPhillips, and Total have developed LedaFlow, a multiphase numerical tool in order to predict multiphase flow phenomena in pipelines. This tool has been extended to handle the rotating wheel geometry using the quasi-3D (Q3D) approach. The Q3D approach compromises speed and accuracy by averaging the flow over transversal slices and is described in more detail below. This approach will also be compared to full 3D simulations carried out using a

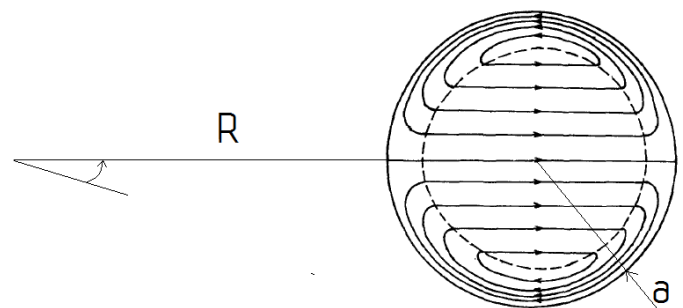


Figure 2: Secondary flow at large Dean number ($De = Re\sqrt{\frac{a}{R}}$), Mori and Nakayama (1964).

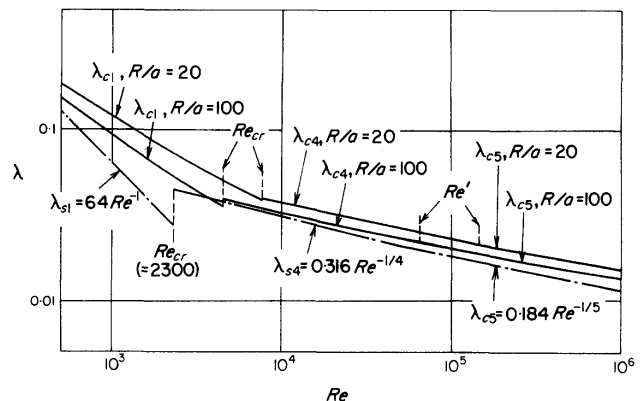


Figure 3: Friction factor as a function of Reynolds number Re for different R/a , Mori and Nakayama (1966).

commercial CFD software, as explained later on.

MODEL DESCRIPTION

Quasi-3D model (Q3D)

The model and numerical method, together with some applications have been described previously in Laux et al. (2007; 2008b; 2008a), Ashrafiyan et al. (2011) and Mo et al. (2014). The model is based on a multi-field concept where mass and momentum equations are formed for all fields in question. This means that for 3-phase flows we normally deal with 9 fields and for 2-phase flow with 4 fields. In our case the mass and momentum equations for each phase are obtained by merging all the fields of a phase into a common transport equation. This process introduces simplifications of the physics but also reduces the solver requirements since the number of equations is reduced. The turbulence is modeled using a $k - \ell$ model where k is the turbulent kinetic energy and ℓ is a turbulent length scale (Laux et al. 2007). Transport equations for turbulent kinetic energy is solved for each phase while the turbulent length scales are solved by a Poisson equation, using a length scale boundary condition at the walls and the large scale interfaces. The sizes of the dispersed fields (bubbles and droplets) are represented by evolution equations for the Sauter mean diameter. The large scale interfaces (LSIs) are reconstructed from the predicted phase volume fractions without solving an own transport equation for fraction functions. At each side of the LSI the model behaves as an Euler-Euler model with a continuous phase containing possible dispersed phases. At the LSI the momentum exchange between the continuous fluids (phases) is computed from standard wall functions for rough walls, see e.g. Ashrafiyan and Johansen (2007). The roughness of the large scale interface is computed by a Charnock model (1955). The same type of wall functions are used to represent the wall boundary conditions (wall friction).

Finally, the model is simplified by assuming small variation over the slices. This allows slice averaging the equations over the transversal dimension (z) of the pipe, as illustrated in Figure 4, thereby reducing the spatial dimensionality. This is important in order to reduce computational time significantly without sacrificing too much of the physics. In addition the model allows for vertical pipe bends. The bends are composed of bend segments with constant radius of curvature. This approach is therefore very well adapted to handle the wheel geometry. In each of the bent segments we use local spherical coordinates, which after the slice averaging is reduced to 2D polar coordinates. The numerical methods applied in this work have been explained previously in Laux et al. (2007). The temporal discretization is first order implicit Euler, while the spatial discretization is using the total variation diminishing (TVD) compliant third order scheme ACUTER (Meese, 1998).

Wheel

The simulation domain is sketched in Figure 5. The geometry has the shape of a wheel with radii ratio $R/a = 40$. For our cases the wheel is filled with two fluids. The wheel and fluids are initially at rest. When the simulation is started the wall velocity is either ramped up or set instantaneously to a given rotation velocity $U^{\text{wall}}(r) = (r/R)U_0^{\text{wall}}$. During the simulations the wall shear stress is directly calculated. The

torque is then given by:

$$T = \int dA^{\text{wall}} \tau^{\text{wall}}(r, \theta) r \quad (1)$$

where $dA^{\text{wall}} = dA^{\text{wall}}(r, \theta)$ is the differential wall area. For Q3D the total torque at a given time is then calculated based on the wall shear stress for each slice as:

$$T = \sum_{i=1}^{N_x} \sum_{j=1}^{N_y} \tau_{j,i}^{\text{wall}} A_{j,i}^{\text{wall}} (R - a + y_j) \quad (2)$$

where (j, i) is cell index across and along the pipe respectively and N_y, N_x is the number of cells in the given directions. Also $\tau_{j,i}^{\text{wall}}$ is the shear stress and $A_{j,i}^{\text{wall}}$ is the slice wall area (two sides) for the given Q3D slice.

If the wheel radius R is large compared to the pipe radius a the following approximation can be used:

$$T \approx 2\pi a R^2 \int_0^{2\pi} \tau_{1D}^{\text{wall}}(\theta) d\theta \quad (3)$$

Using 1D-collapsed Q3D variables (cross-sectionally averaged) we get:

$$T \approx R \sum_{i=1}^{N_x} \tau_{1D,i}^{\text{wall}} A_{1D,i}^{\text{wall}} \quad (4)$$

where $\tau_{1D,i}^{\text{wall}}$ is the 1D collapsed wall shear stress in 1D-cell i and $A_{1D,i}^{\text{wall}}$ is the wall area for this 1D-cell.

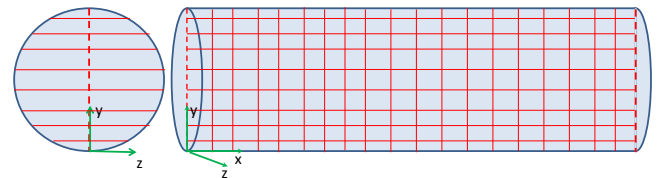


Figure 4: Grid layout of a pipe. The model equations and predicted field quantities are averaged over the slices seen in left part of the figure.

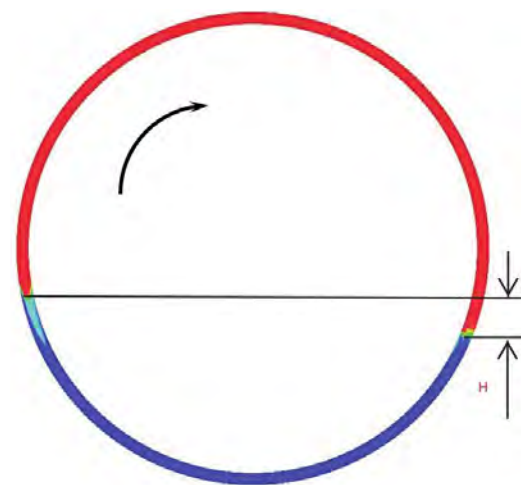


Figure 5: Sketch of a $R = 1$ m radius wheel made of $d = 5$ cm diameter pipe. Here the wheel is filled with approximately (40%, 60%) of heavy 'blue' and light 'red' phases respectively.

Fluent's VOF model (3D)

Fluent 14.5 was used to simulate the full 3D wheel geometry. We employed the compressive volume of fluid method (VOF) to simulate the two-phase flow phenomena. The VOF method uses a color function, F , to capture the phase fractions and identify the free surface position. The color function is defined as a step function which represents the volume fraction of one of the fluids within each cell. When F is equal to 0 or 1 the cell is away from the interface and the cell is fully filled with one phase, while for values between 0 and 1 the cell is filled with both phases and therefore the cell contains a free surface. VOF belongs to the so called one-fluid family of methods, where a single momentum equation is solved for the domain and the resulting velocity field is shared among the phases. Additionally, in cases where the interface is clearly defined (segregated array of phases – as seen in Fig. 5) good predictions are expected. On the other hand, in the case that dispersions are formed, the VOF model does not perform well. In that case, as will be shown later, coupling with an Euler-Euler approach is desired. Due to $Re \sim 10^4$ in several cases, the turbulence needs to be considered, and modeled by means of the Reynolds Averaged Navier-Stokes equation and the realizable $k-\epsilon$ model. The latter solves two additional transport equations for the turbulent kinetic energy and the dissipation rate. A complete description of the method and the governing equations can be found in Fluent Theory Guide by ANSYS, Inc (2013).

Experimental setup

The Wheel Flow Loop consists of a 5.25 cm inner diameter stainless steel pipe bent into a 1 m radius wheel shaped loop which gives a total volume of 13.4 litres. The wheel used in the current tests can be operated at 250 bar of pressure and is placed inside a climate chamber for temperature control from -5 to $+60$ °C. Furthermore, the wheel has a shorter section consisting of a sapphire pipe for visual observations of phenomena inside the wheel. There is a video camera attached to the wheel which follows it during rotation and thus can capture videos from all positions.

The wheel is instrumented with temperature sensor PT100, pressure sensor and a Shaft Type Reaction Torque Transducer from Sensotec with a range up to 135 N.m. Additionally, filling of the wheel is done by high pressure pumps outside the wheel chamber and all components, liquids and gases, are filled by weight with an accuracy of ± 5 g. As will be shown later, experiments using different mixtures were performed: air/water, oil/water and oil/gas with significant CO_2 content. For CO_2 cases, the amounts filled of each compound are given in Table 1.

Table 1: Mass composition of CO_2 experiment

Compound	Amount [g]	Mass fraction [%]
CO_2	676	8%
CH_4	965	12%
Oil	6479	80%

At 60 °C this gave a pressure of 250 bar. The wheel was rotated at various velocities ranging from 0.05 m/s to 2 m/s as for the 3D and Q3D simulations. Experiments were performed at temperatures ranging from 25 °C to 55 °C with steps of 10 °C between. The other experiments were run at

approximately standard conditions.

RESULTS

In this work several cases involving the three different mixtures have been selected for comparison of experimental data with numerical results obtained by the classic VOF method and our Q3D approach. The properties of air, water and oil are listed in Table 2. Additionally, different meshes of our wheel were generated for Fluent's VOF and LedaFlow-Q3D simulations.

Table 2: Fluid properties at $P = 1$ bar and $T \approx 20$ °C

	Air	Water	Oil
Density [kg/m^3]	1.2	1000	800
Viscosity [Pa.s]	1.9E-5	1.0E-3	3.2E-3

Some numerical simulations using Fluent were performed with two different meshes. The coarse mesh is composed of ≈ 80000 cells while the refined mesh has a total of ≈ 230000 cells. The difference in the calculated torque on the two meshes was less than 2%. The coarse mesh provides sufficiently accurate results with less computational effort; therefore the coarse mesh was adopted for the subsequent simulations. The Q3D approach used less cells, approximately 5000.

As seen in Figure 6, the steady-state is reached for both simulations ($t > 12$ s) even though initial conditions are quite different. For instance, at the beginning Fluent imposes *instantaneously* full velocity generating a high torque to spin the wheel.

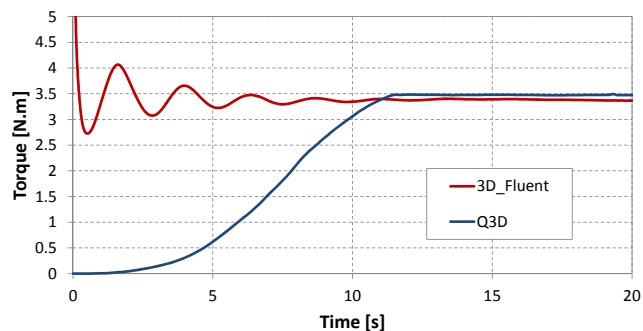


Figure 6: Transient evolution of torque for Fluent and Q3D.

In Q3D the wall velocity was slowly increased in order to help convergence, unlike the Fluent's VOF which did not evidence any problem related to convergence when using a step velocity.

It should be noted that, for calibration purposes, a constant offset was applied to ensure that experimental torque vanishes at zero velocity for all mixtures. For instance, an offset 0.49 N.m was applied in air/water mixture, while 0.37 N.m in oil/water mixture. Furthermore, due to uncertainties and current limited understanding of experimental torque oscillations, we try to focus on the comparison of qualitative flow behaviour in the Wheel. As further work, improvement of raw data treatment, as well as Wheel balancing, will be assessed, since in some cases standard deviation can reach

up to 1.75 N.m.

Air and water mixture $\alpha_W = 40\%$

The first mixture is composed of 60% air and 40% water. Here different velocities are imposed and torque measured for each velocity. The height H shown in Figure 5 will balance the torque needed to rotate the wheel and is correlated to wall shear stress. Visual comparison between LedaFlow-Q3D and Fluent's VOF showed that H values are very similar.

For none of the cases, carry-over was predicted and main contribution of torque is due to water phase. Figure 7 shows that numerical results are below experimental data with a maximum difference around 1.2 N.m at 2 m/s. Furthermore, Fluent's VOF and LedaFlow-Q3D presented very similar results in cases where the interface is clearly identified, evidencing the prediction capabilities of both tools, although Q3D uses significantly less cells. Regarding computational effort, Fluent's VOF took 4.5 hours over 6 cores, while LedaFlow-Q3D spent approximately 2 hours over 2 cores in order to simulate 20 seconds.

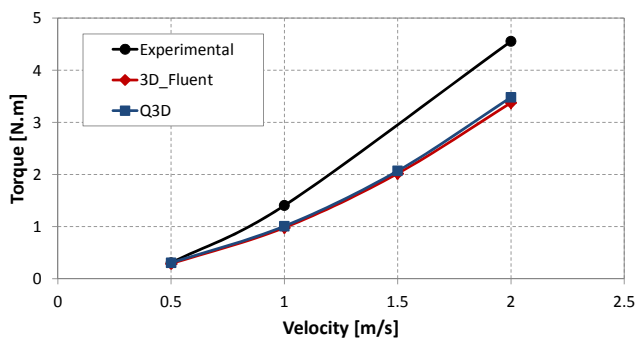


Figure 7: Torque versus velocity for air-water mixture.

Oil and water mixture $\alpha_W = 50\%$

Oil and water composes the second mixture, filling the wheel evenly. Due to small difference between densities, one phase carries the other, generating emulsions when velocity is above 1 m/s.

According to Figure 8, torque also increases with velocity and is still underestimated. For instance, at the maximum velocity 1 m/s the Q3D result is 0.7 N.m below experimental, while the difference between Fluent's VOF and experimental results is 0.8 N.m.

CO₂ mixtures $\alpha_{CH_4-CO_2} = 22.2\%$

The molar composition of gas in the third mixture is 15.3% CO₂, 61.3% CH₄ among other components (mass composition is detailed in Table 1), with GOR = 220 m³/m³. An increasing-decreasing stepwise rotation velocity is imposed to the wheel at different pressure-temperature conditions as seen in Figure 9. Comparison between lab data and numerical results of torque versus wheel velocity is presented in Figures 10 and 11. Notice that error bars represent the standard deviation around the mean torque value indicating a transient effect due to changes in the velocity, evidencing oscillations in torque for some points.

However, points with small deviation do not show bars.

Experimentally, it is observed that torque increases with velocity until a certain velocity is reached and liquid starts to be carried over, causing a sudden drop in torque. When deceleration begins, lower torque values are measured and hysteresis is clearly evidenced.

Q3D results showed that hysteretic behaviour is predicted

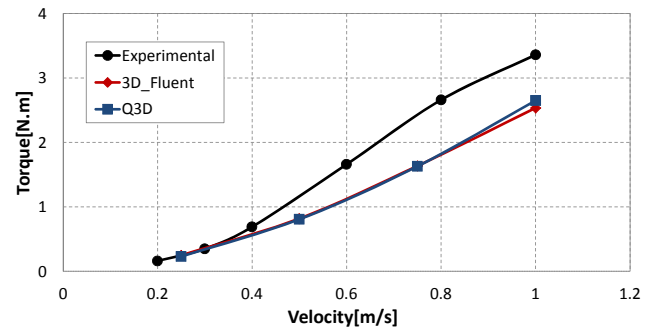


Figure 8: Torque versus velocity for oil-water mixture.

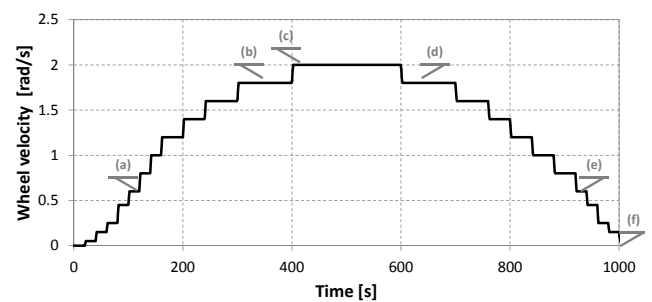


Figure 9: Stepwise velocity imposed to the wheel.

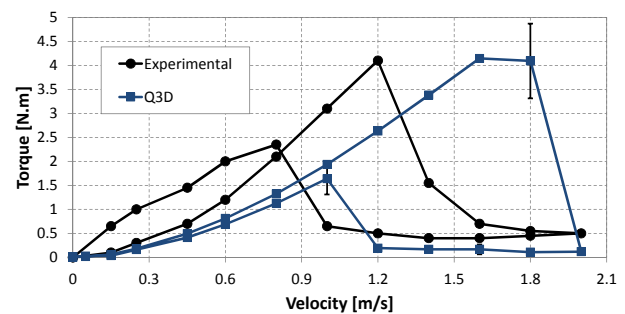


Figure 10: Torque versus velocity for CO₂ mixture at $P = 182.4$ bar and $T = 15.3$ °C.

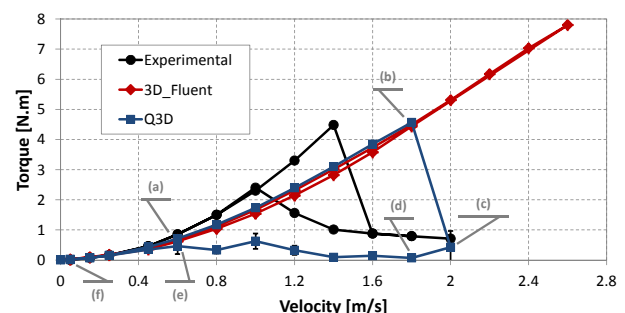


Figure 11: Torque versus velocity for CO₂ mixture at $P = 250$ bar and $T = 60$ °C.

qualitatively when the particle size equation is solved (i.e. VOF coupled with an Euler-Euler approach with dynamic of particle size) and coalescence time is increased to delay formation of larger bubbles which separate out of the liquid phase. Moreover, Figure 10 shows in detail that the predicted velocity needed to cause torque drop differs in 0.6 m/s from experimental, whereas in Figure 11, the difference is 0.4 m/s. Thus, the numerical model underestimates the torque needed for a given velocity and carry over starts at higher velocity than observed in experiments.

On the other hand, as expected the results obtained with Fluent's VOF did not present the abrupt drop in torque and hysteretic behaviour, because the dynamics of particle size is not modelled in VOF.

Figure 12 shows phase distribution at different times. Notice that each snapshot is related to Figures 9 and 11 showing how the wheel velocity evolves and the associated average torque for each velocity. When the wheel accelerates, liquid is carried over through the gas cap region and fine bubbles progressively entrains the liquid front. After $t = 402$ s the interface completely vanished (the gas phase is fully dispersed in the liquid) causing a torque drop as shown at $t = 650$ s. Then, as wheel velocity decreases, bubbles start to coalesce and eventually the gas cap is restored, generating a small torque recovery.

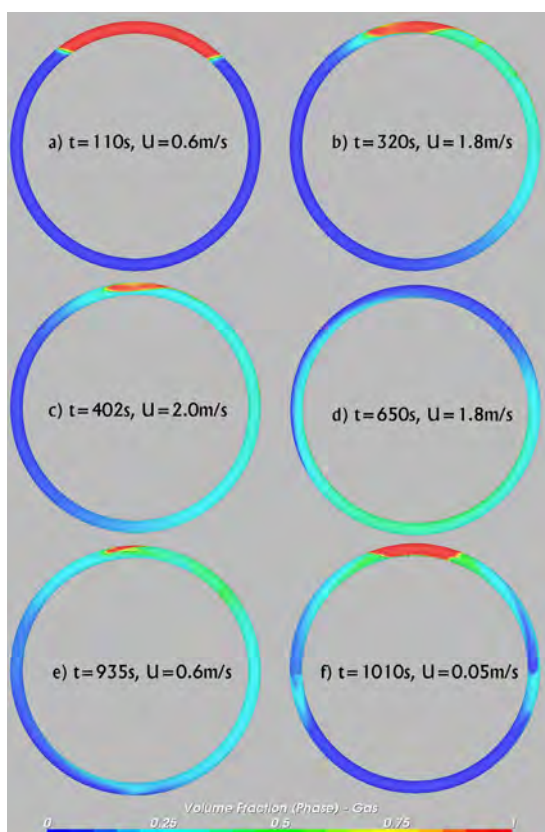


Figure 12: Results from Q3D approach for a CO₂ mixture at different velocities – clockwise direction ($P = 250$ bar and $T = 60$ °C).

CONCLUSION

The conclusions are:

1. Numerical results using LedaFlow-Q3D approach and Fluent's VOF were compared with lab data for three different mixtures. Predictions are generally below experimental data in all cases. Qualitatively, both VOF and Q3D are able to reproduce the torque dependence on wheel velocity. And, Q3D is able to predict the drop in torque for high velocities.
2. In cases where the interface is defined and phases segregated, there is a close agreement between Fluent's VOF and LedaFlow-Q3D results.
3. Relative error between VOF and Q3D is below 4% and may be considered insignificant when taking into account that Q3D simulations were faster and used less cells. The minor importance of secondary flow (3D effect) for the radii ratio $R/a = 40$ and flow regime may explain the close agreement.
4. Dynamic treatment of dispersed phase particle size is a critical element to reproduce the hysteresis on torque.

Current work is focused on mitigating the difference between experimental and numerical results. In particular, the large oscillations in torque measurements need to be further understood. Finally, a coupled VOF-Multi Fluid approach in Fluent, including droplet size modeling, will be compared to the Q3D results.

ACKNOWLEDGEMENT

The financial support to the Leda Project, the long-time contributions from the Leda Technical Advisory Committee, as well as permission to publish, by Total, ConocoPhillips, and SINTEF are all gratefully acknowledged. Our colleagues Ernst Meese, Runar Holdahl, and Jørn Kjølås (SINTEF), Wouter Dijkhuizen and Dadan Darmana (Kongsberg Oil & Gas Technologies), Harald Laux (OSRAM Opto Semiconductors GmbH, Regensburg), and Alain Line (INSA, Toulouse) are acknowledged for their contributions to the development.

REFERENCES

- ALMEIDA, A.S. *et al.* (2010). "CCGS opportunities in the Santos basin pre-salt development". Society of Petroleum Engineers, Rio de Janeiro, Brazil.
- ANSYS (2013). "14.5 Fluent Theory Guide". ANSYS, Inc.
- ASHRAFIAN, A. and JOHANSEN, S. (2007). "Wall boundary conditions for rough walls". *Progress in Computational Fluid Dynamics*, **7**(2-4), 230–236.
- ASHRAFIAN, A. *et al.* (2011). "Multidimensional modeling of stratified wavy three-phase flows". *Rio Pipeline Conference & Exposition*, Sep. 20-22.
- CHARNOCK, H. (1955). "Wind stress on a water surface". *Quart. J. Roy. Meteor. Soc.*, **81**, 639–640.
- JOHNSEN, E.E. *et al.* (2001). "A simplified experimental approach for measuring viscosity for water-in-crude-oil emulsions under flowing conditions". *J. Dispersion Science and Technology*, **22**, 33–39.
- JOHNSEN, E. and RØNNINGSEN, H. (2003). "Viscosity of 'live' water-in-crude-oil emulsions: experimental work

and validation of correlations”. *J. Petroleum Science and Engineering*, **38**, 23–36.

LAUX, H. *et al.* (2007). “Simulation of multiphase flows composed of large scale interfaces and dispersed fields”. *Proc. Int. Conf. Multiphase Flows, Leipzig, July 9-13th*.

LAUX, H. *et al.* (2008a). “Multi-dimensional simulations of slug and slug-like flows in inclined pipes and channels”. *6th North American BHRG Conference on Multiphase Technology*. Banff, Canada.

LAUX, H. *et al.* (2008b). “Multidimensional simulations of multiphase flow for improved design and management of production and processing operation”. *2008 Offshore Technology Conference*. Houston, Texas, U.S.A. OTC-19434.

MEESE, E.A. (1998). *Finite volume methods for the incompressible Navier–Stokes equations on unstructured grids*. Ph.D. thesis, NTNU.

MO, S. *et al.* (2014). “Quasi-3d modelling of two-phase slug flow in pipes”. *The Journal of Computational Multiphase Flows*, **6**, 1–12.

MORI, Y. and NAKAYAMA, W. (1964). “Study on forced convective heat transfer in curved pipes (1st report, laminar region)”. *Int. J. Heat Mass Transfer*, **8**, 67–82.

MORI, Y. and NAKAYAMA, W. (1966). “Study on forced convective heat transfer in curved pipes (2nd report, turbulent region)”. *Int. J. Heat Mass Transfer*, **10**, 37–59.

RASCH, A. *et al.* (2001). “Evaluation of a low dosage hydrate inhibitor in hydrocarbon fluid systems at high subcooling”. *Presented at 10th International Conference Multiphase '01*, 13–15. Cannes, France.

URDAHL, O. *et al.* (1997). “Viscosity measurements of water-in-crude-oil emulsions under flowing conditions: A theoretical and practical approach”. *Colloids and Surface A: Physicochemical and Engineering Aspects*, **123**, 623–634.

WHITE, D. and BOND, J. (1971). “A low shear rate turbulent flow apparatus”. *Applied Scientific Research*, **23**, 368–372.

ZAIN, Z. *et al.* (2001). “Evaluation of CO₂ gas injection for major oil production fields in malaysia - experimental approach case study: Dulang field”. *Presented at SPE Asia Pacific Improved Oil Recovery Conference*, Kuala Lumpur, Malaysia.